Research Article

Study of PEM Fuel Cell End Plate Design by Structural Analysis Based on Contact Pressure

Tapobrata Dey,[1] **Jaydeep Deshpande**,[2] **Debanand Singdeo**,[1] **and Prakash C. Ghosh**[1]

[1]*Department of Energy Science and Engineering, Indian Institute of Technology Bombay, Mumbai 400076, India*
[2]*Department of Mechanical Engineering, Virginia Polytechnic Institute and State University, Blacksburg, Virginia 24060, USA*

Correspondence should be addressed to Tapobrata Dey; tapobrata.dey@gmail.com

Received 9 August 2018; Revised 27 November 2018; Accepted 29 November 2018; Published 2 January 2019

Academic Editor: Ciro Aprea

A fuel cell stack is configured to power any load ranging from watts to megawatt by varying cells connected in series. During stack assembly, major emphasis must be placed on application of adequate external pressure for reducing the ohmic losses, the purpose of which is to achieve proper contact between the cell components and minimize the contact resistance. Present work aims to study the influence of geometry of the cell, bolt configuration, gasket thickness mismatch, and material properties of different components of average and distribution contact pressure. The geometries are evaluated for end plate designs with a view to understand the pressure distribution and contact resistance in each case. Among different designs, extruded hexagon is found to perform well with an average contact pressure of 0.13 MPa and contact resistance of 28 Ω-cm^2. Greater gasket thickness requires higher forces to be applied before the GDL makes contact with BPP. The effect of gasket thickness mismatch is evaluated for different values to identify its appropriate value. The pressure is applied using bolts and position and number of bolts is determined for homogeneous contact pressure on the active area. This study provides a framework for future end plate design of fuel cells.

1. Introduction

Polymer electrolyte membrane fuel cell (PEMFC) is one of the promising technologies for electrical power generation. Presently, PEMFCs utilize solid polymer membrane as an electrolyte and porous carbon cloth/paper as electrode. The electrode and electrolyte together are referred to as the membrane electrode assembly (MEA) which is equipped with bipolar plate (BPP) on both the sides for reactant flow and current collection. A number of such units (single cells) are connected in series and are flanked by endplate at both ends to form a fuel cell stack. Graphite is usually the material of choice for bipolar plates due to its high corrosion resistance but still lighter material is preferred for the endplate [1, 2]. PEMFC has received considerable attention, especially in the automotive sector as the low operating temperature ($< 100^{\circ}$C) allows quick start-up and portability [3, 4].

Depending upon the application, PEMFC stack has to endure a wide range of deformation and stresses. Behaviour of the fuel cell stack under these stresses is primarily governed by the material properties of its components. In this respect, the role of the stack clamping pressure is also significant. It holds the assembly together and ensures leak-proof operation of stack. In most cases, it is accomplished by using bolting arrangement across the cell area. The force applied in this manner is responsible for achieving better contact between the electrode and bipolar plate. Uneven and inadequate contact pressure can severely inhibit cell performance and can eventually lead to component failure of the stack. This effect is more pronounced for larger stack dimensions and it becomes necessary to optimize the contact pressure exerted. At higher normal forces, the contact between adjacent cell components improves. However, increased pressure also causes an increase in the mass transport losses in the cell, incurred due to gas diffusion layer (GDL) compression [5]. Nonhomogeneous externally applied load on the end plates also affects the spatial pressure distribution on the active area. This in turn is related to the geometrical structure of the end plate and thus presents scope for further improvement by design modification. Many researchers have studied the effect

induced due to bolting on MEA [6, 7]. Additionally, some have focused on the deformation of stack components, i.e., membrane and bipolar plate [7, 8].

The importance of using adequate load during fuel cell assembly is reflected in its ohmic dominated region of the performance characteristics. The observed potential drop cannot be explained on the basis of bulk material conductivity alone. The additional drop is attributed to contact resistance which originates due to current flow across the interfaces between different cell components. Contact resistance is found to be directly related to the compressive force applied across it. For rectangular cell design, experiments show near to zero contact pressure at the centre of the active area irrespective of clamping method [9]. Moreover, irregular pressure distribution on the GDL also results into nonuniform contact resistance values. Various methods have been employed by researchers to improve the contact pressure distribution and different correlations between pressure distribution and clamping torque have been suggested [10–17]. Zhang et al. used an approach for finding out the experimental relation between clamping pressure and contact resistance [18]. Attempts have been made to experimentally quantify the pressure distribution variation with different clamping forces [19]. One of the preferred procedures to apply clamping force is bolt tensioning. However, bolt placements induce the contact region to be located around them. These are as possess contact pressure gradients, thereby producing nonuniform pressure distributions for larger cell assemblies. Bates et al. analysed performance of single cell and a stack of 16 cells with an applied pressure in range 0.5 to 2.5 MPa [9]. It was pointed out that pressures below 0.5MPa do not affect the pressure distribution significantly. In the same evaluation, they also confirmed the compressive pressure on the GDL to be ~1MPa. Moreover, Bates et al. also highlighted the need to study the effect of contact pressure distribution with reference to contact resistance as a primary reason for cell performance degradation [9].

Montanini et al. studied the pressure distribution on the MEA and gasket by using piezoresistive sensor arrays for varying clamping torque from 5Nm to 10Nm, producing a range of contact pressure from 0.339MPa to 1.46MPa. The significance of end plate curvature and deformation has been highlighted in their work [19]. Similar studies have shown that the maximum applicable torque is 15.8 Nm, beyond which membrane shows plastic behaviour during its deformation under the applied stresses [6].

Wen et al. studied performance of PEMFC stack under various configurations using different number of bolts and varying their positions [20]. In the same study, it has been also reported that larger contact pressure yields higher power density irrespective of configuration, number of bolts, and applied torque. Zhou et al. showed the effect of surface irregularities and nonuniformities in bipolar plate and MEA with contact pressure distribution [11]. In another study, they have established a numerical model of contact resistance [21] based on bipolar plate microscopic surface topology and GDL structure simulation. The microscale model thus developed can effectively predict contact resistance for any given pair of GDL and bipolar plate in contact if their structural and material properties are known appropriately. Asghari et al. studied end plate design for 5 kW fuel cell [22], in which consideration is given to material selection and developing finite element model. The model was further selected to calculate deflections and stresses under applied loads and thickness optimization. Although the criteria for material selection and end plate design have been mentioned, detailed study of end plate design and contact pressure distribution needs to be carried out.

On the basis of literature and to the best of the author's knowledge, studies related to contact pressure highlight appropriate assumption of complete contact between GDL and BPP while performing finite element method based analysis. However, while using off the shelf gasket, thickness of the GDL and sealing gasket may not be equal, resulting in an initial no-contact zone between BPP and GDL. Ismail et al. have justified the need of studying contact pressure between GDL and BPP in presence of sealing gasket after studying the contact resistance for BPP coated with PTFE [7].

The objective of present work was to evaluate a number of different end plate design and configuration for fuel cell applications. The key parameter for the analysis was the contact pressure distribution over active area under an applied force using finite element analysis on *ANSYS*® platform. Experimental validation was carried out to support the modelling results. The model is used to explore the effect of gasket thickness mismatch and bolt placement configuration on contact pressure distribution. Study is accompanied by a detailed stress analysis of all components pertaining to the modified stack. The analysis is found to be helpful in predicting regions of high and low mechanical stresses, which are useful in predicting sites of failure. Thus, this study aims at optimization of the clamping force, structure, and configuration for better contact pressure distribution.

2. Numerical Methodology

2.1. Description of Geometry. The geometry considered in the simulation includes the end plates, two bipolar plates, two gaskets, two GDLs, and a membrane. GDLs are joined to the membrane as nonseparable entities. As in common assembly procedure, the membrane is placed in the middle, with GDL on each side, followed by the gasket. This assembly is sandwiched between the bipolar plates and is enclosed by the end plates as shown in Figure 1. In the geometry analysis ten bolts are considered with two configurations, one is with all bolts outside the graphite plates and the other one is with all bolts inside the graphite plates.

Geometries have been created in *SOLIDWORKS* and are imported in *ANSYS® Academic Research, Release 14.0 workbench*. Materials assigned are as shown in the Table 1. The flow channels of the bipolar plate are not included. Gasket material is selected as PTFE. GDL material is selected as carbon paper as it gives good performance due to high porosity (>70%) [6]. The clamping bolts considered are supposed to have standard M10 specifications. While evaluating the geometries, only the change in its external shape is considered, the total physical volume of the plate being kept constant. Reference end plate for the study is as depicted in Figure 1.

Table 1: Material properties of PEMFC components.

Descriptions	Materials	Young's Modulus (GPa)	Poisson's ratio	Density (kgm^{-3})
End Plate	SS316	193	0.3	8000
	Aluminium Alloy	71	0.33	2770
	Titanium Alloy	96	0.36	4620
Current Collector	Copper	120	0.34	8960
Bipolar Plate	Graphite	10	0.3	1500
GDL	Carbon Cloth	10	0.25	400
Membrane	Nafion®	0.19	0.25	2000
Gasket	PTFE	1	0.46	2200
	Silicone Rubber	0.05	0.47	2300
Bolt/Nut	Stainless Steel	180	0.3	8600

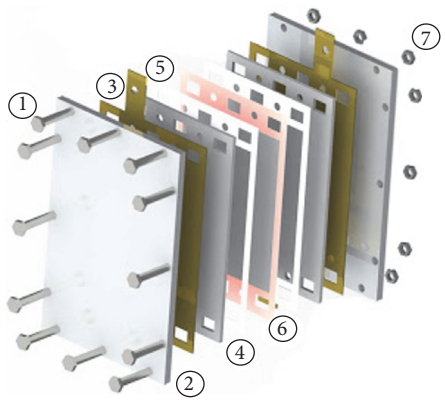

1: Bolt
2: End Plate
3: Current Collector
4: Bipolar plate
5: Gasket
6: Membrane
7: Nut

Figure 1: Schematic geometry of PEMFC.

It is found that pressure gradient occurs across the GDL due to bolting at the cell edges, especially in the case of large cell area [23]. To improve upon this shortcoming, modified end plate surfaced designs have to be considered. Commonly used end plates possess flat surfaces as shown in Figure 1. Improvement of pressure distribution can be carried out by compensating for low pressure zone in the centre portion of the cell by changes in end plate geometry. Following are the various geometries which are considered in this study to evaluate the best suited end plate as shown in Figure 2.

(i) Plain (flat) end plate
(ii) Extruded triangles
(iii) Extruded H shape
(iv) Cut triangles
(v) Cut H shape
(vi) Hexagonal pattern

Case 1 (evaluation of geometry). The size of end plate in our study is 300x200 mm^2. Graphite plate, gasket, membrane, and current collector are each of dimension 267 × 172 mm^2. Active area for all geometries is constant and it is equal to 199x154 mm^2. All design features on end plates have same height of extrusion or cut 2 mm.

Case 2 (effect of number of bolts and position and its effect on contact pressure distribution). After obtaining the results of Case 1, the selected geometry is subjected to analysis in order to determine the effect bolt number and their arrangement. For this purpose, a total of four placement schemes are considered comprised of 4 bolts, 8 bolts, 10 bolts, and 12 bolts, while treating the total force as a constant. Thus, the force on individual bolt is changed for each configuration.

For each of these schemes, the spacing between the adjacent bolts for each side of the end plate is given by

$$d = \frac{L}{n+1} \quad (1)$$

where "d" is the distance between adjacent bolts, "L" is the edge length, and n is the number of bolts.

Case 3 (analysis of pressure distribution considering that the bolt passes through the bipolar plate). After completing the analysis in Cases 1 and 2, the geometry and number and bolts are selected. The bolt position is then shifted such that it lies inside the bipolar plate and the change in pressure distribution is determined.

Case 4 (evaluation of the effect of gasket thickness). In most of the previous studies, the BPP is assumed to be in perfect contact with GDL while performing the FEA. However, in most practical scenarios, there is some difference between the gasket and GDL thickness. This mismatch produces an initial no-contact region between BPP and GDL, when compressive forces are gradually applied. As a result, the applied force is initially, spent primarily in compressing the gasket to the level where the bipolar plate just starts touching the GDL. Once this occurs, any higher applied force is transferred to the GDL resulting in contact at a certain pressure between the GDL and bipolar plate. The application of higher forces causes the GDL and gasket to deform together. The contact pressure in

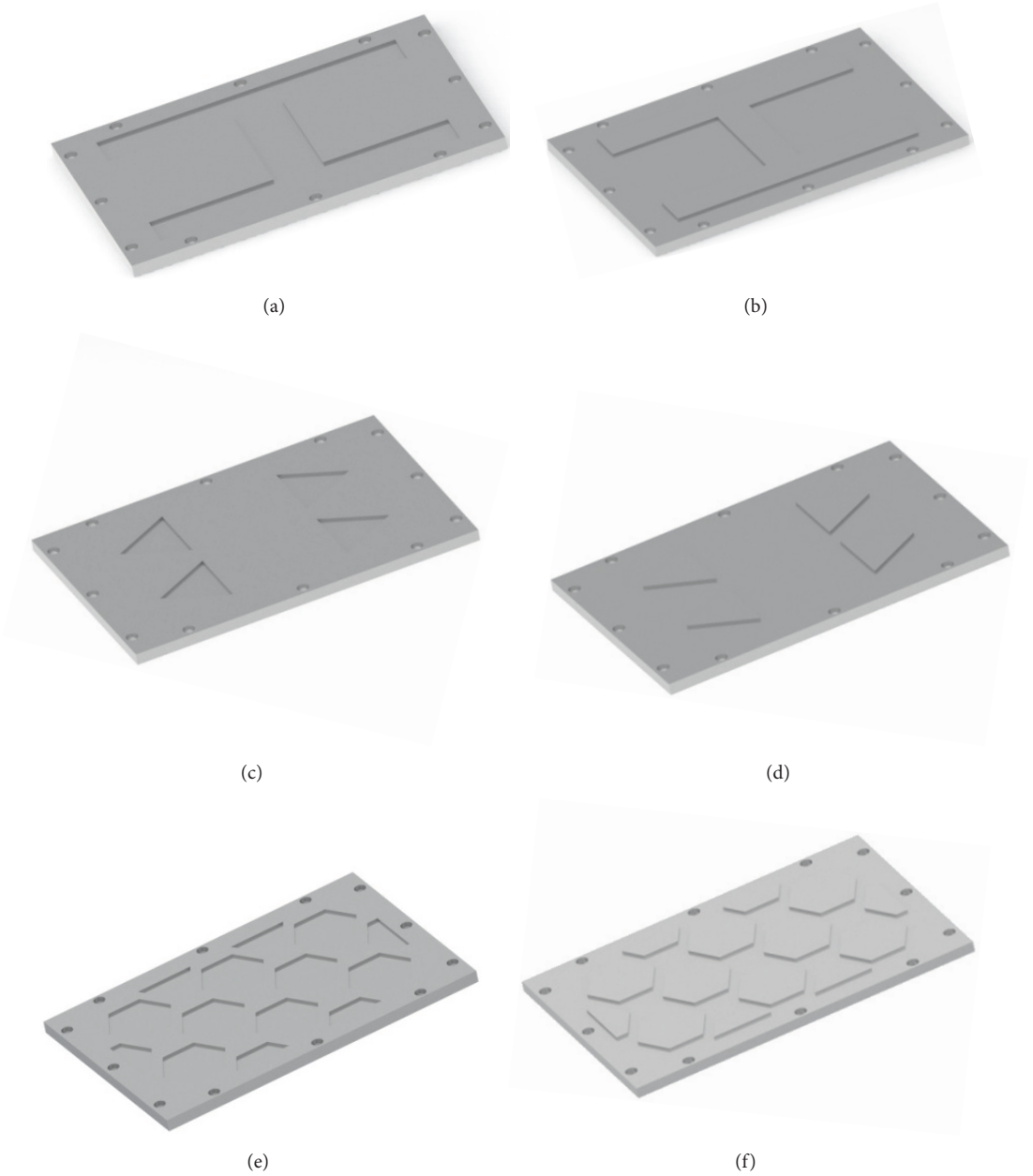

Figure 2: Different end plate design.

such a scenario can be represented a function of difference between gasket thickness and GDL thickness.

$$P_c = f(\Delta x) \tag{2}$$

where the mismatch parameter Δx = (gasketthickness) – (GDLthickness); P_c is the contact pressure.

The final geometry obtained after three successive case studies is subjected to further analysis for evaluating the effect of change in the gasket thickness. Gasket thickness is changed in three equal steps from 0.1 to 0.2 mm, keeping the thickness of GDL constant (0.4mm).

Case 5 (evaluation of different end plate materials). The influence of the end plate material on the pressure distribution, stresses, and deformation is investigated using different materials. It is implemented using the configuration chosen after analysing the result of the previous cases.

2.2. Boundary Condition. In some reported works [6, 24], a simplified 2D domain is chosen and appropriate boundary conditions are applied to simulate real cell loading. But such a model may fail to predict effects arising from multiaxial stress and out of plane effects. Therefore, in this study the assembly is modelled as it is with exact replication of the real assembly.

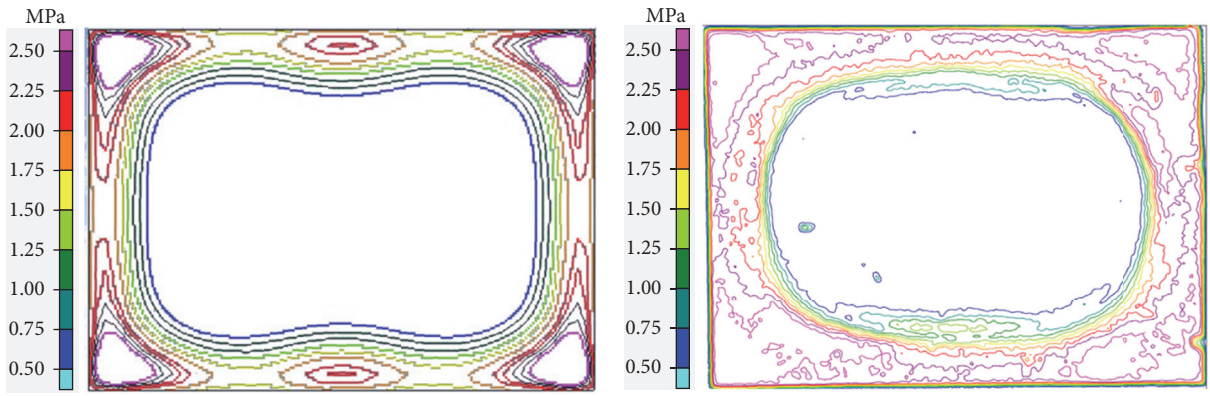

Figure 3: Pressure contour plot obtained using (a) simulation and (b) experimental technique.

The GDL is fixed to the Nafion® layer by means of "Nonseparable" joint condition. In-plane motion of GDL is partially restricted, since membrane is constrained to move in-plane and only perpendicular motion is allowed. All neighbouring plates have "bonded" type condition and so as to prevent penetration of members into other bodies, intermediate bonded conditions are specified. This allows restricted deformation as observed in practical scenarios. Contacts are carefully modelled to avoid unphysical behaviour. The study also encompasses complex scenarios such as multipoint linkages of the bolts and multicontacts. The use of certain logical approximations allows the solution to be simplified in such cases.

Assessment of different geometry is carried by converting the applied torques into axial forces on all bolts. The force is applied on the surface of the bolt, normal to the plane of the PEMFC, and is directed inwards. The force on the structure can be applied either by direct load on face or by means of bolt tensioning. Bolt tensioning in practical cases is achieved by applying torque on the bolts. However, such a case can lead to certain abnormalities in the results due to unavailability of exact friction coefficients. Therefore, it is prudent to convert the applied moment into equivalent axial force. The applied value of pressure on the bolts depends on the tightening torque. The actual clamping force depends on stiffness of bolt material, deflection of end plate, stiffness of end plate, friction between bolt threads and nut threads, thread profile, etc. But, to simplify calculation, clamping force in our study is obtained using following relation [25]:

$$F = \frac{T}{KD} \tag{3}$$

where T is the tightening torque, F is the clamping force, D is the bolt diameter, and K is the bolt friction factor. The friction factor value (0.43) accounts for surface roughness, friction and deformation of the bolts during tightening. From simulation, the total deformation, equivalent stress, and maximum principal stress data can be extracted from all cases.

2.3. Material Properties. Material properties assigned to the individual components are as per Table 1. To evaluate the effects of change in end plate material on the pressure distribution, three different materials have been specifically chosen namely steel, aluminium alloy, and titanium alloy.

3. Solution Procedure

The solid-mechanics model is developed for the geometry using the commercial FEM software ANSYS® Academic Research, Release 14.0. In the next step, loads and boundary conditions are applied according to the cases discussed above. Contact tools and deformation tools are used as output data generators in each of the cases, and after solving the equations, results are postprocessed and plotted as per requirements. The convergence criteria for all the calculations have been set as 10^{-7}.

4. Result and Discussions

The geometry required for modelling has been modelled and its various aspects are investigated. The effect of contact pressure distribution is clearly narrated in this section.

4.1. Contact Pressure Distribution for Plain Plates. Pressure distribution on the MEA is obtained both experimentally and numerically for 20 Nm applied torque, as shown in Figures 3(a) and 3(b). Experimental validation has been carried out using a fuel cell with SS-316 end plates and bipolar plates made of graphite. The carbon paper based MEA is sandwiched between the two bipolar plates, with a pressure sensitive film inserted between them. The pressure sensitive film used is Fuji Film PRESCALE, Japan (LW and LLW). The pressure plots obtained are analysed using the software suit FPD 8010E.As seen in Figure 3(a), contact pressure in the central zone is much less than that near the edges. Similar behaviour is also confirmed in our numerical analysis results as shown in Figure 3(b). The result obtained by simulation is found to be in agreement with the experimental results within 6.5% variation.

4.2. Effect of End Plate Geometry on Contact Pressure. After validation, the model is further used to assess the impact of different end plate geometries on the contact pressure distribution and average contact pressure is evaluated for a force amounting to 25 kN and gasket mismatch of 0.2 mm. Transfer of the axial force is found to alter with modification in the surface geometry, causing a distinct pressure profile in each case. During numerical simulations, only a fraction of these nodal points which represent the participating bodies in FEM has been found to play a role in contact during the application of compressive pressures. The participating nodes can be identified by their nonzero contact pressure values. These points are then chosen and subject to further analysis. To carry out a qualitative comparison of the different end plate designs, the percentage of nodes which has the same pressure magnitude is compared for different geometries. The motivation behind adopting this method is that the comparison should be independent of the number of nodes. However, care should be taken to ensure that the discretization allows satisfactory solution and convergence. Also, it is to be noted that the choice of y-axis in Figure 5 has been made with the intention of comparing the effect of different end plate geometries on the distribution of compressive pressures among the points participating in contact. As the cut-hexa geometry has the highest percentage of nodes within at a compressive pressure of ~ 0.5 MPa, its y-axis range has also been used for other geometries for comparative study purpose.

From the Figure 4(a), it can be seen that the conventionally used end plate design, i.e., the flat plain end plate, has several numbers of nodes in the low pressure region. Thus, the average contact pressure obtained for the flat plate design is 0.06 MPa, which is on the lower end compared to other designs. The end plate with hexagonal cuts shows similar pressure distribution as obtained with the plain design, consisting of large percentage of nodal points in the low pressure region of 0.02 to 0.1 MPa. The error bar indicates a wide variation from the mean value with respect to maxima and minima which points towards nonuniform pressure distribution. Thus, although the hexagonal cut pattern is uniform over the entire plate, it does not result into a uniform distribution. The plain and hexagonal cut geometry only differs in the spatial pressure distribution of pressure, which is clearly evident from the contour plots in Figures 4(a) and 4(b). The average contact resistance for hexagonal cut geometry has a value nearly 58Ω cm^2 (Figure 6). The end plate with cut triangles shows better distribution (0-0.4 MPa) and higher average pressure than the flat plate or hexagon cut end plate as shown in Figure 4(d). This results into lower contact resistances within of 0-50Ω cm^2, with the average contact resistance being ~ 32Ω cm^2. Even better contact pressure distribution is found from the simulation results for the extruded hexagon type end plate as shown in Figure 4(c). The higher average pressure is obtained and these can be inferred from the nodal percentage distribution plot in Figure 5, which shows large percentage of nodes distributed in medium to high pressure region (0-0.3 MPa). The least deviation from the mean pressure is observed in case of extruded hexagonal geometries, which indicates of a good contact pressure distribution all over the contact surface. Contact resistance range of 0-30Ω cm^2 with an average value of 28Ω cm^2 is noted for this configuration. The extruded triangles geometry shows concentration of higher contact pressure around the triangulations. Still, the distribution is found to be uniform across the whole pressure range as seen in Figure 4(e). Although the distribution is uniform, the contact resistance plot in Figure 6 shows the contact resistance range across the GDL to be 0-50 Ω cm^2, with the average contact resistance ~32 Ω cm^2. Among all geometries, extruded triangle has better prospect as large percentage of nodes lie in the medium or high pressure zones. Referring to Figure 4(f), for Cut H type configuration, majority of the points lie in the region with contact pressure < 0.1 MPa; thus the overall contact pressure yields a lower value. Similarly, the contact resistance at the BPP-MEA interface is in the range of 0-90Ω cm^2 (Figure 6). The average contact resistance lies ~ 60Ω cm^2. However, extruded H geometry performs better as shown in Figure 4(g) with an average pressure of ~ 0.12 MPa and average contact resistance of ~ 51Ω cm^2.

Thus, over plain and cut end plates, end plates with extrusions are more suitable for obtaining uniform contact pressure profiles and higher average contact pressure. It also has the potential to reduce the plate thickness and can benefit in terms of weight reduction.

4.3. Effect of Number of Bolts on Contact Pressure. The number of bolts is intuitively expected to be another significant parameter while applying a certain clamping force. To carry out the study, four different arrangements have been chosen, where the number of bolts used are varied from 4 to 12 as shown in the Figure 7. While placing the bolts, the emphasis is kept on maintaining the symmetry in the bolt positions.

In Figure 8, the effect of number of bolts and their positions on contact pressure distribution is shown. It is found that the average contact pressure as well as contact pressure distribution is affected by the number of bolts used and their locations. Increasing the number of bolts is found to improve the uniformity of contact pressure distribution. From Figure 9(a), it is noted that lower average contact pressure results in case of 4 bolts. This can be accounted due to higher localized force at the bolt location, which produces significantly higher pressures only around the zone of bolt placement. This leads to a contact pressure distribution which is less uniform (Figure 8(a)). The increase of bolt number to 6 and subsequently to 8 is seen to alleviate the effect, resulting in improvement in the pressure distribution. But, increasing of the number of bolts beyond 10 does not offer any significant advantage. It can be concluded that the configuration comprised of 10 bolts gives a good contact pressure distribution and better average contact pressure.

4.4. Effect of Bolt Placement through the Graphite Plates. One of the commonly used configurations for placing bolts is to place all of them outside the graphite plates. It causes bending of the end plates, and some of the energy is lost in bending of bolts. This reduces the contact pressure on

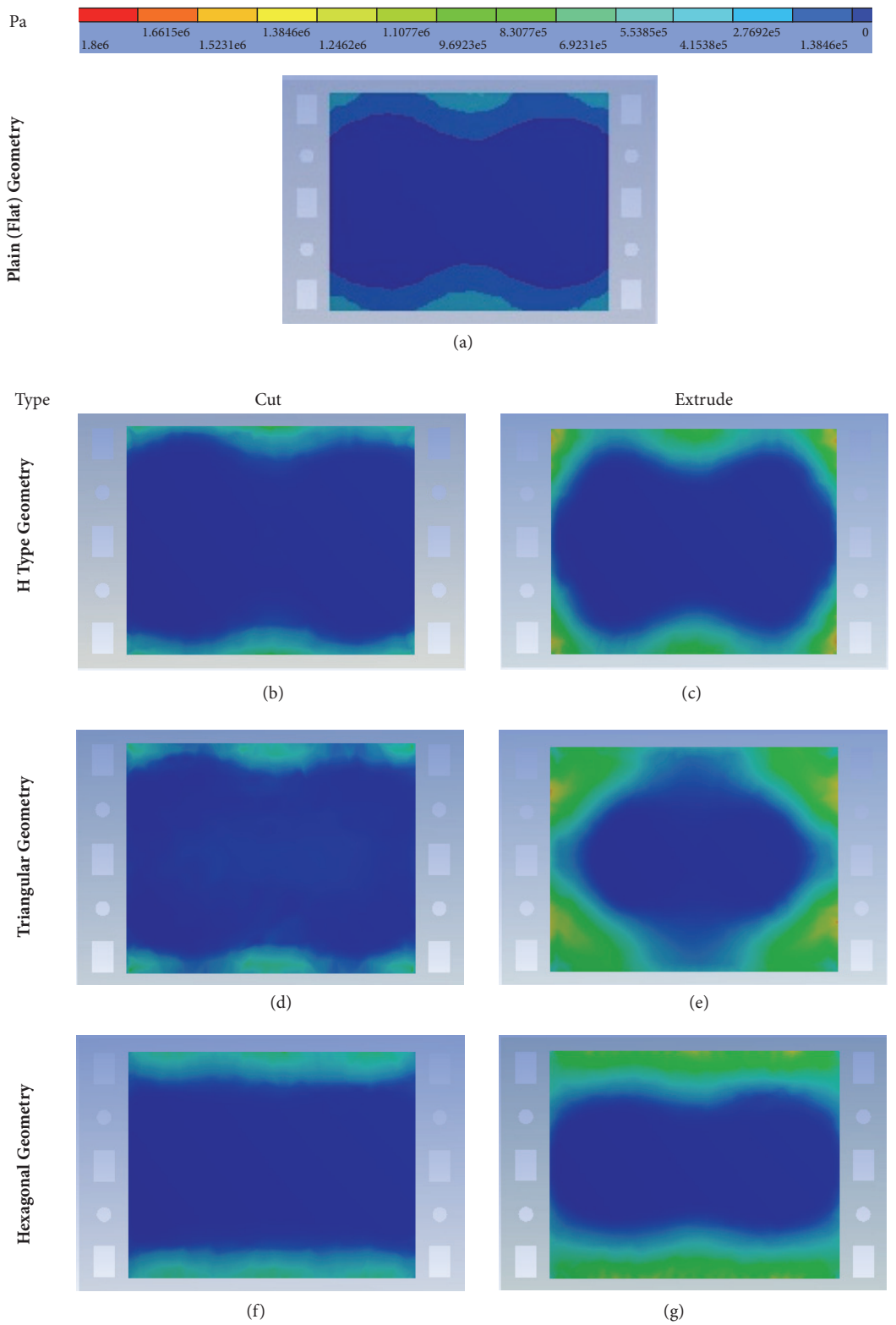

Figure 4: Contact pressure distribution on GDL surface at 25 kN.

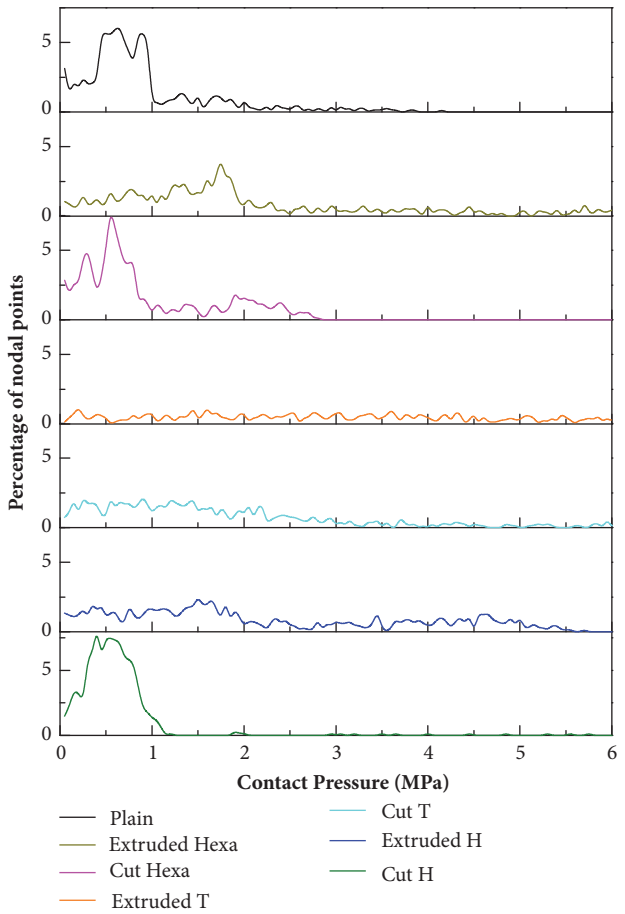

Figure 5: Percentage of node points versus compressive pressure for different end plate geometries.

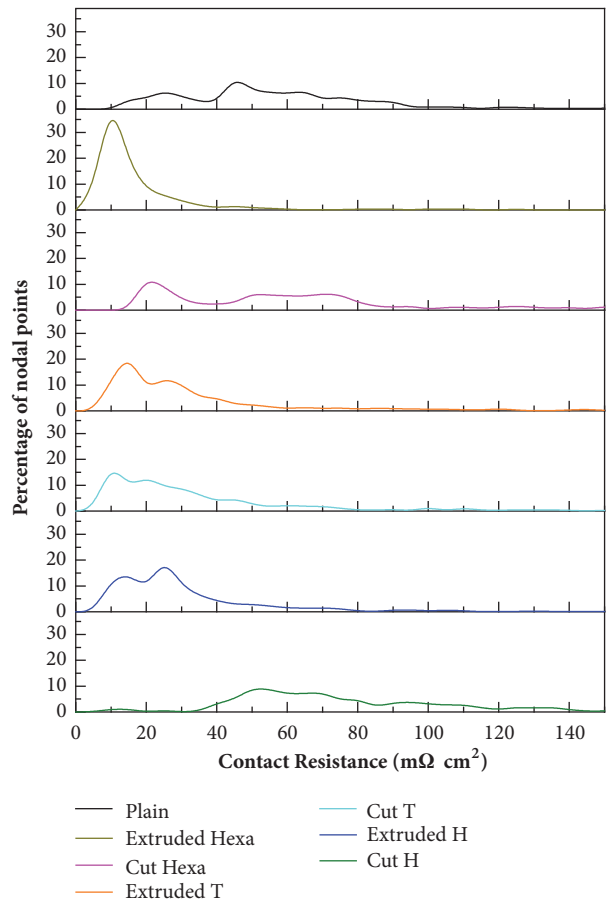

Figure 6: Percentage of node points versus contact resistance for different end plate geometries.

GDL. Thus, another option where all bolts pass through the graphite plates has to be considered. Figures 9(b) and 9(c) show the contact pressure distribution comparison for two different cases: one with all bolts inside and the other when they are kept outside. It can be clearly seen that including all bolts inside has improved the contact pressure distribution and average contact pressure as well. This not only reduces bending of end plates and bolts but also improves the overall strength of the stack.

4.5. Effect of Gasket Thickness on Contact Pressure. The choice of gasket thickness is also important and should be carefully studied before proceeding towards stack assembly. In the current work the impact of having a 0.4 mm gasket of Teflon material with mismatch parameter ranging from 0.1 to 0.2mm is analysed. It is found that at higher gasket thickness, i.e., at low mismatch parameter value, a major component of the applied pressure is directly transferred to the GDL. Thus, the average compressive pressure on the gasket is lower for a mismatch factor of 0.1 mm as shown in Figure 9(d). Increasing the mismatch factor to 0.15 mm causes a shift in the pressure distribution between the GDL and the gasket, with more pressure being transferred to the gasket and lesser to the GDL. The higher pressure causes further compression of the gasket. To ensure leak-proof operation of the fuel cell, it is desired that the gasket is in a fully compressed state. At even higher mismatch factor value (0.2 mm), similar pressure values on the gasket is noticed, indicating that pressure on the gasket has reached a threshold value. Thus, a mismatch factor of 0.15–0.2 mm is relevant for fuel cell stack applications.

5. Conclusion

PEMFC offers a promising solution to our future power needs of a compact, reliable, and modular source. This technology is vying for commercialization and had already found its way into automobile and aerospace applications. Stack architecture of the fuel cell is found to have an important role from both performance and commercialization point of view. The current study shall act as a guideline for future fuel cell design activities, since it provides a comprehensive solution for ensuring homogeneous pressure distribution, leakage proof operation, and improving performance. Several end plate geometries were considered in this study, along with number of bolts used in tightening and their position with respect to the cell. Extruded hexagonal geometry for end plate shows better distribution of contact pressure. Number of bolts is found to have a significant impact on average contact pressure and distribution. In the study, it is found

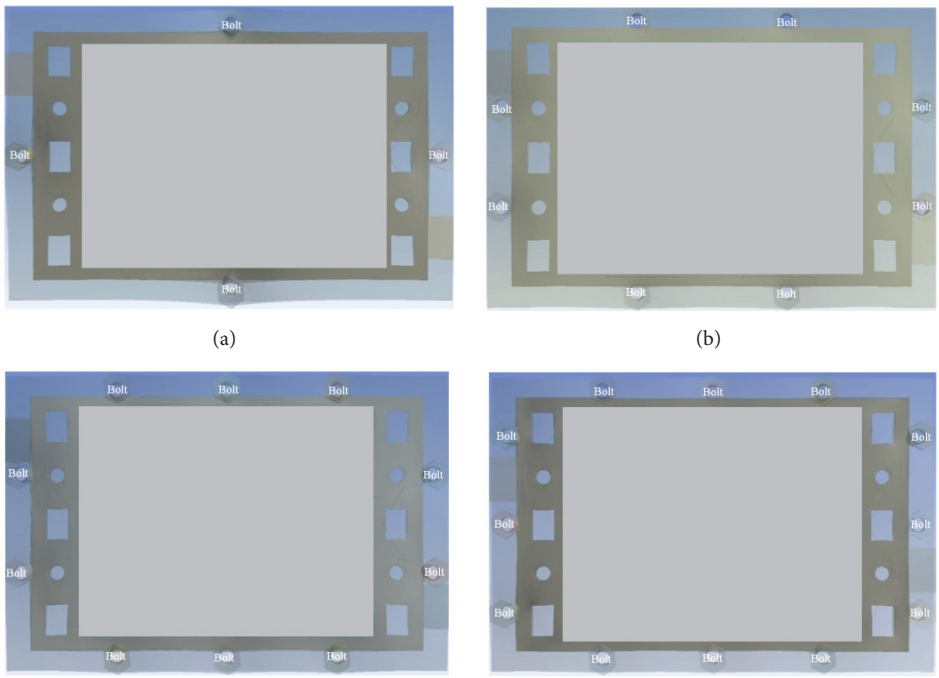

Figure 7: The position of different bolts with respect to the cell assembly of numbers {(a) 4 bolts, (b) 8 bolts, (c) 10 bolts, and (d) 12 bolts} for estimating the contact pressure distribution.

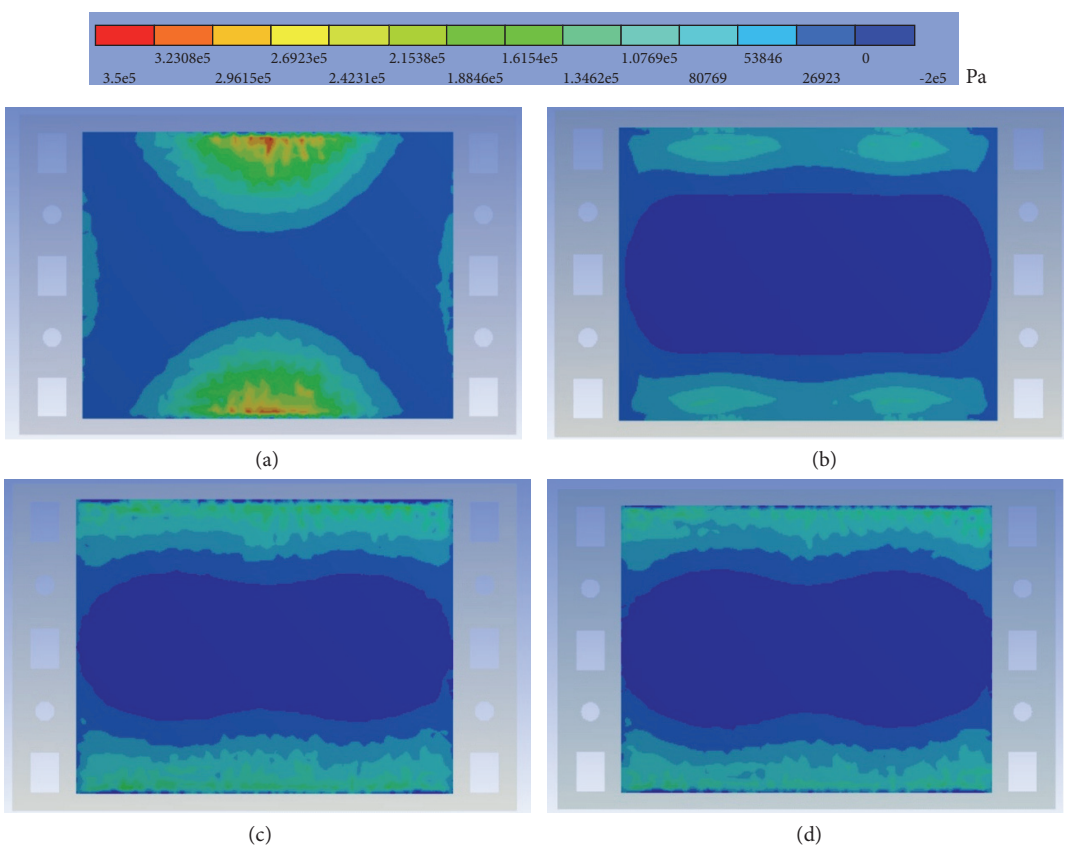

Figure 8: Effect of different number of bolts {(a) 4 bolts, (b) 8 bolts, (c) 10 bolts, and (d) 12 bolts} on contact pressure distribution.

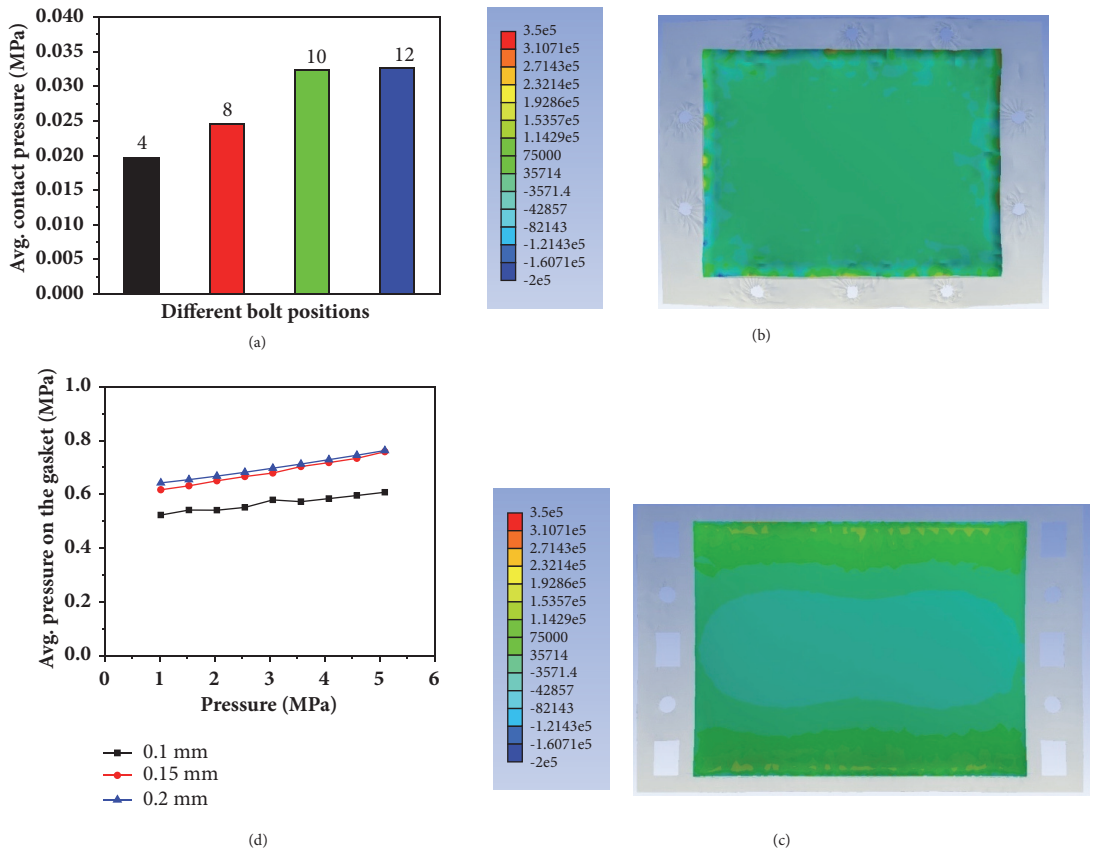

FIGURE 9: (a) Effect of different number of bolts on the average contact pressure; (b) effect of bolt placement through plates on contact pressure distribution of all bolts inside and (c) outside; (d) variation of average gasket compression with different applied pressure.

that 10 bolts are suitable for obtaining uniformity for the structure under study. Bolt placement also has a considerable impact on the average contact pressure and contact pressure distribution, i.e., by placing all bolts through the graphite plate has contributed to more uniform contact pressure distribution. Another important aspect of cell assembly is to choose a gasket thickness complementary to thickness of the GDL for a given compressive pressure. The evaluations of gasket thickness from this study shall provide insights into the permissible gasket thickness. It is found that the difference between GDL and gasket is tolerable between 0.15 mm to 0.2mm. Thus, by optimizing geometry, number of bolts, their position, and gasket thickness, average contact pressure of ~ 0.8 MPa is obtained at a bolt loading of 8–10 Nm. Change in material is found to be of lesser importance. However, lighter materials like aluminium alloys can be effectively utilized, producing weight savings of ~65% while retaining better contact pressure distribution.

Nomenclature

d: Distance between adjacent bolts (mm)
D: Bolt diameter (mm)
F: Clamping force (N)
K: Bolt friction factor
L: Edge length (mm)
n: Number of bolts
P_c: Contact pressure (MPa)
T: Tightening torque (N m).

Abbreviations

BPP: Bipolar plate
GDL: Gas diffusion layer
LW: Low pressure
LLW: Super low pressure
MEA: Membrane electrode assembly
PEMFC: Polymer electrolyte membrane fuel cell
PTFE: Polytetrafluoroethylene
2D: Two dimensional.

Data Availability

The data used to support the findings of this study are available from the corresponding author upon request.

Disclosure

The present address of Tapobrata Dey is Department of Mechanical Engineering, D Y Patil College of Engineering, Akurdi, Pune 411044. The present address of Debanand

Singdeo is Department of Energy Technology, Aalborg University, Pontoppidanstraede 101, Denmark.

Conflicts of Interest

The authors declare that they have no conflicts of interest.

References

[1] B. C. Steele and A. Heinzel, "Materials for fuel-cell technologies," *Nature*, vol. 414, no. 6861, pp. 345–352, 2001.

[2] J. Zhang, J. Wu, H. Zhang, and J. Zhang, *Pem Fuel Cell Testing and Diagnosis*, Elsevier, Oxford, UK, 2013.

[3] R. O'Hayre, S-.W. Cha, W. Colella, and B. F. Prinz, *Fuel Cell Fundamentals*, John Wiley & Sons, Oxford, UK, 2nd edition, 2009.

[4] M. Ji and Z. Wei, "A review of water management in polymer electrolyte membrane fuel cells," *Energies*, vol. 2, no. 4, pp. 1057–1106, 2009.

[5] W.-K. Lee, C.-H. Ho, J. W. Van Zee, and M. Murthy, "Effects of compression and gas diffusion layers on the performance of a PEM fuel cell," *Journal of Power Sources*, vol. 84, no. 1, pp. 45–51, 1999.

[6] D. Bograchev, M. Gueguen, J.-C. Grandidier, and S. Martemianov, "Stress and plastic deformation of MEA in fuel cells. Stresses generated during cell assembly," *Journal of Power Sources*, vol. 180, no. 1, pp. 393–401, 2008.

[7] M. S. Ismail, D. B. Ingham, L. Ma, and M. Pourkashanian, "The contact resistance between gas diffusion layers and bipolar plates as they are assembled in proton exchange membrane fuel cells," *Journal of Renewable Energy*, vol. 52, pp. 40–45, 2013.

[8] A. Oyarce, N. Holmström, A. Bodén, C. Lagergren, and G. Lindbergh, "Operating conditions affecting the contact resistance of bi-polar plates in proton exchange membrane fuel cells," *Journal of Power Sources*, vol. 231, pp. 246–255, 2013.

[9] A. Bates, S. Mukherjee, S. Hwang et al., "Simulation and experimental analysis of the clamping pressure distribution in a PEM fuel cell stack," *International Journal of Hydrogen Energy*, vol. 38, no. 15, pp. 6481–6493, 2013.

[10] T. Dey, D. Singdeo, M. Bose, R. N. Basu, and P. C. Ghosh, "Study of contact resistance at the electrode-interconnect interfaces in planar type Solid Oxide Fuel Cells," *Journal of Power Sources*, vol. 233, pp. 290–298, 2013.

[11] P. Zhou, P. Lin, C. W. Wu, and Z. Li, "Effect of nonuniformity of the contact pressure distribution on the electrical contact resistance in proton exchange membrane fuel cells," *International Journal of Hydrogen Energy*, vol. 36, no. 10, pp. 6039–6044, 2011.

[12] X. Wang, Y. Song, and B. Zhang, "Experimental study on clamping pressure distribution in PEM fuel cells," *Journal of Power Sources*, vol. 179, no. 1, pp. 305–309, 2008.

[13] D. Singdeo, T. Dey, and P. C. Ghosh, "Contact resistance between bipolar plate and gas diffusion layer in high temperature polymer electrolyte fuel cells," *International Journal of Hydrogen Energy*, vol. 39, no. 2, pp. 987–995, 2014.

[14] Y. Zhou, G. Lin, A. J. Shih, and S. J. Hu, "A micro-scale model for predicting contact resistance between bipolar plate and gas diffusion layer in PEM fuel cells," *Journal of Power Sources*, vol. 163, no. 2, pp. 777–783, 2007.

[15] A. Kraytsberg, M. Auinat, and Y. Ein-Eli, "Reduced contact resistance of PEM fuel cell's bipolar plates via surface texturing," *Journal of Power Sources*, vol. 164, no. 2, pp. 697–703, 2007.

[16] W. R. Chang, J. J. Hwang, F. B. Weng, and S. H. Chan, "Effect of clamping pressure on the performance of a PEM fuel cell," *Journal of Power Sources*, vol. 166, no. 1, pp. 149–154, 2007.

[17] S. Lee, C. Hsu, and C. Huang, "Analyses of the fuel cell stack assembly pressure," *Journal of Power Sources*, vol. 145, no. 2, pp. 353–361, 2005.

[18] L. Zhang, Y. Liu, H. Song, S. Wang, Y. Zhou, and S. J. Hu, "Estimation of contact resistance in proton exchange membrane fuel cells," *Journal of Power Sources*, vol. 162, no. 2, pp. 1165–1171, 2006.

[19] R. Montanini, G. Squadrito, and G. Giacoppo, "Measurement of the clamping pressure distribution in polymer electrolyte fuel cells using piezoresistive sensor arrays and digital image correlation techniques," *Journal of Power Sources*, vol. 196, no. 20, pp. 8484–8493, 2011.

[20] C.-Y. Wen, Y.-S. Lin, and C.-H. Lu, "Experimental study of clamping effects on the performances of a single proton exchange membrane fuel cell and a 10-cell stack," *Journal of Power Sources*, vol. 192, no. 2, pp. 475–485, 2009.

[21] P. Zhou, C. W. Wu, and G. J. Ma, "Influence of clamping force on the performance of PEMFCs," *Journal of Power Sources*, vol. 163, no. 2, pp. 874–881, 2007.

[22] S. Asghari, M. H. Shahsamandi, and M. R. Ashraf Khorasani, "Design and manufacturing of end plates of a 5 kW PEM fuel cell," *International Journal of Hydrogen Energy*, vol. 35, no. 17, pp. 9291–9297, 2010.

[23] S. Karvonen, T. Hottinen, J. Ihonen, and H. Uusalo, "Modeling of polymer electrolyte membrane fuel stack end plates," *Journal of Fuel Cell Science and Technology*, vol. 5, no. 4, 2008.

[24] X. Lai, D. Liu, L. Peng, and J. Ni, "A mechanical-electrical finite element method model for predicting contact resistance between bipolar plate and gas diffusion layer in PEM fuel cells," *Journal of Power Sources*, vol. 182, no. 1, pp. 153–159, 2008.

[25] R. G. Budyanas and J. K. Nisbett, *Shigley's Mechanical Engineering Design*, The McGraw-Hill Companies, 2012.